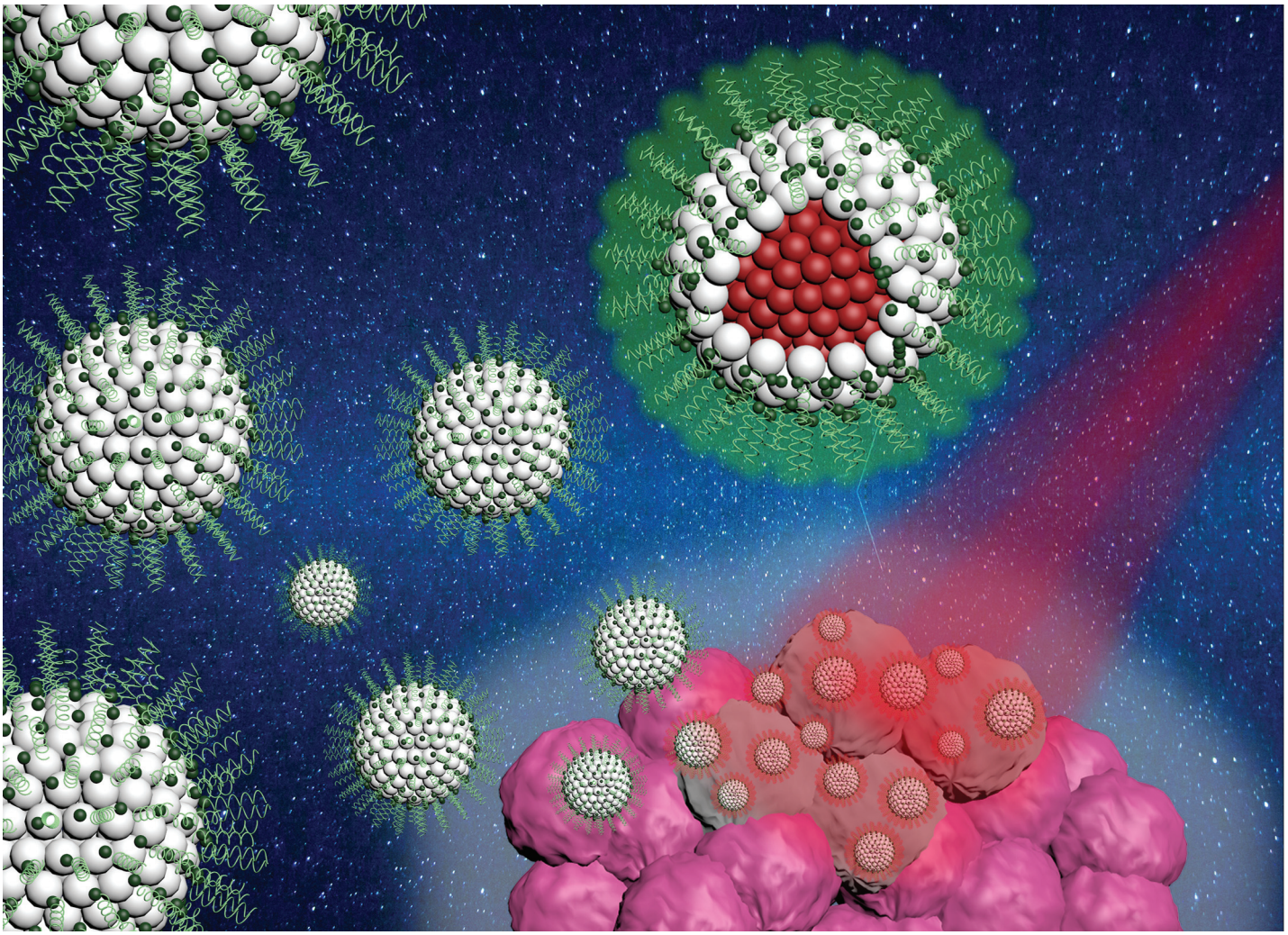

Showcasing research from the State Key Laboratory of Luminescence and Application, Changchun Institute of Optics, Fine Mechanics and Physics, Chinese Academy of Science, Changchun, China.

An 800 nm driven $NaErF_4$@$NaLuF_4$ upconversion platform for multimodality imaging and photodynamic therapy

This illustration depicts the nanostructure of the $NaErF_4$@$NaLuF_4$-Ce6/PEG upconversion nanosystem and the scheme of its 800 nm driven photodynamic therapy. The nanosystem solves the problem of the mutual influence of multimodality imaging within a simple core/shell structure. Therefore, this nanosystem can serve well as a theranostic agent for multimodality imaging and image-guided therapy.

As featured in:

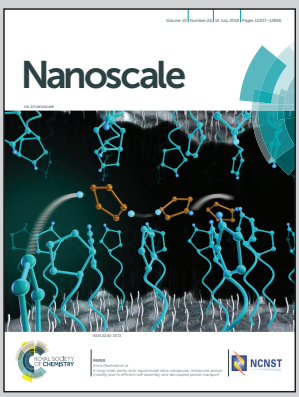

See Yulei Chang, Xianggui Kong *et al.*, *Nanoscale*, 2018, **10**, 12356.

ROYAL SOCIETY OF CHEMISTRY

rsc.li/nanoscale

Registered charity number: 207890

Published on 04 April 2018. Downloaded by Changchun Institute of Optics, Fine Mechanics and Physics, CAS on 8/8/2019 8:17:54 AM.

Nanoscale

PAPER

View Article Online
View Journal | View Issue

Check for updates

Cite this: *Nanoscale*, 2018, **10**, 12356

An 800 nm driven $NaErF_4$@$NaLuF_4$ upconversion platform for multimodality imaging and photodynamic therapy†

Qiqing Li,[a,b] Xiaodan Li,[a,c] Li Zhang,[a,c] Jing Zuo,[a,b] Youlin Zhang,[a] Xiaomin Liu,[a] Langping Tu,[a] Bin Xue,[d] Yulei Chang *[a] and Xianggui Kong *[a]

Received 17th January 2018,
Accepted 22nd March 2018

DOI: 10.1039/c8nr00446c

rsc.li/nanoscale

Multimodality imaging-guided therapy based on lanthanide-doped upconversion nanoparticles (UCNPs) has become a trend in cancer theranostics. However, the overheating effect of 980 nm excitation in photodynamic therapy (PDT) and the difficulties in optimizing multimodality imaging integration within a single particle are still challenges. Herein, 800 nm driven $NaErF_4$@$NaLuF_4$ UCNPs have been explored for optimized multimodality imaging and near-infrared (NIR) triggered PDT. Our results confirmed that the optimal ~5 nm shell thickness can well balance the enhancement of upconversion luminescence and the attenuation of energy transfer efficiency from Er^{3+} towards a photosensitizer, to achieve efficient production of singlet oxygen ($^1O_2$) for PDT under 800 nm excitation. Furthermore, the as-obtained $NaErF_4$@$NaLuF_4$ UCNPs showed effective and applicable performance for upconversion luminescence (UCL) imaging, X-ray computed tomography (CT), and high-field T_2 magnetic resonance imaging (MRI). This nanomaterial can serve as an excellent theranostic agent for multimodality imaging and image-guided therapy.

1. Introduction

Lanthanide-doped upconversion nanoparticles (UCNPs) have attracted extensive attention as promising multimodality contrast agents. They are recognized as having diverse tunable optical properties, excellent magnetic properties, and strong X-ray attenuation. Accordingly, they have emerging applications in upconversion luminescence (UCL) imaging, magnetic resonance imaging (MRI) and X-ray computed tomography (CT).[1–10] Furthermore, after surface modification with functional molecules, *i.e.* photosensitizers or chemo-therapeutic drugs, the obtained nanoplatform is able to serve as a multimodality imaging guided therapeutic system.[11,12] However, when it comes to practical application, there are two main problems: (1) the overheating effect of 980 nm excitation light in therapy[13,14] and (2) the difficulties in optimizing multimodality imaging integration within a relatively simple nanostructure.[15]

First of all, for photo-triggered theranostic applications, Yb^{3+}-sensitized UCNPs under 980 nm excitation are widely used because of their relatively high UCL efficiency. However, 980 nm light can be strongly absorbed by water and biological tissues, which often causes tissue damage as a consequence of the overheating effect. Alternatively, due to the significantly decreased water absorption, 800 nm light excitation has been considered as an ideal candidate to replace 980 nm light excitation due to its less harmful impact on biological tissues. Recently, by utilizing a NIR dye or Nd^{3+} as the sensitizer,[16–20] UCNPs have already shown efficient UC emission under 800 nm excitation. Nevertheless, the stability and hydrophobic properties of the NIR dye are still the main concern when it comes to practical bioapplications. At the same time, the inevitable energy loss during the energy transfer (ET) from Nd^{3+} ions to activators (Er^{3+}) and back-energy transfer processes cause a complex adjustment process. Fortunately, very recently, a new multi-wavelength excitation of a $NaErF_4$ system has been reported.[21–23] A core–shell nanostructure was employed to respond to the ~800 nm, ~980 nm and ~1530 nm light and generate a monochromic red emission (~655 nm), such as $NaErF_4$@$NaYF_4$ ($NaLuF_4$ or $NaGdF_4$). Importantly, due to the heavily doped activators of Er^{3+}, the $NaErF_4$ core is sensitive to the surrounding environment and an inert shell is needed, which means the thicker the shell, the stronger the UC luminescence. However, a very thick shell is negative for luminescence resonance energy transfer (LRET) based applications,

[a]State Key Laboratory of Luminescence and Applications, Changchun Institute of Optics, Fine Mechanics and Physics, Chinese Academy of Sciences, Changchun 130033, China. E-mail: xgkong14@ciomp.ac.cn, yuleichang@ciomp.ac.cn
[b]University of the Chinese Academy of Sciences, Beijing 100049, China
[c]The First Hospital of Jilin University, Changchun 130021, China
[d]Key Lab of Optoelectronics Devices and Systems of Ministry of Education/Guangdong Province, Shenzhen University, Shenzhen 518060, China
†Electronic supplementary information (ESI) available. See DOI: 10.1039/c8nr00446c

This journal is © The Royal Society of Chemistry 2018

Published on 04 April 2018. Downloaded by Changchun Institute of Optics, Fine Mechanics and Physics, CAS on 8/8/2019 8:17:54 AM.

such as PDT.[24] Therefore, a newly developed 800 nm driven material system has been attached to study the LRET efficiency between the UCNPs and acceptors for further practical applications.

For the bio-imaging applications, lanthanide elements benefiting from 4f electron configurations provide UCNPs with significant paramagnetic properties for MRI and strong X-ray attenuation for X-ray CT. Combined with UCL imaging, the UCNPs as multimodality contrast agents have been applied for diagnostic and imaging-guided therapy.[25–27] However, there is a conflict among these imaging functions because the overall performance of UCNPs in multimodality imaging is not equal to a simple collection of various imaging functional elements from every single component. For example, the traditional $NaYF_4$:20% Yb,2% Er UCNPs perform with an efficient UCL, but low X-ray attenuation for CT and almost no MRI ability. In contrast, to enhance the MRI ability, it requires high concentrations of magnetic ions, such as Dy^{3+} and Gd^{3+} ions, which would efficiently quench the UCL in most cases. Interestingly, the strategy of coating $NaErF_4$ with a $NaLuF_4$ shell will solve these obstacles simultaneously. The heavily doped Er^{3+} ions in $NaErF_4$@$NaLuF_4$ not only provide efficient UC emissions but also possess a large intrinsic magnetic moment ($9.59\mu_B$) and K-edge energy (57.49 keV).[28–30] Furthermore, by combining the large K-edge energy (63.3 keV) of Lu^{3+} ions[3] in the shell, the $NaErF_4$@$NaLuF_4$ nanoparticle will improve the imaging ability of the UCL and X-ray CT.

Herein, a $NaErF_4$@$NaLuF_4$ nanostructure was synthesized and applied to tri-modality (UCL, CT and MR) imaging-guided photodynamic therapy. The sufficient Er^{3+} ions in the core of the nanosystem enable the combination of robust upconversion luminescence, large X-ray absorption, and high transverse relaxation rate ($1/T_2$). In order to produce singlet oxygen ($^1O_2$) for PDT, the as-prepared UCNPs were further conjugated with chlorin e6 (Ce6) photosensitizer through covalent bonding. Therefore, the relationship between the shell thickness and singlet oxygen generation was further studied in detail. Moreover, the $NaLuF_4$ shell can not only improve the UCL intensity but also enhance the X-ray CT imaging ability. Therefore, by utilizing the $NaErF_4$@$NaLuF_4$ upconversion system, we obtained a favourable tri-modality imaging probe. Our results demonstrate that such a design affords a potential strategy to induce an Er^{3+} singly doped nanosystem for imaging-guided therapy applications.

2. Experimental section

2.1 Reagents

$ErCl_3{\cdot}6H_2O$ (99.9%), $LuCl_3{\cdot}6H_2O$ (99.9%), oleic acid (90%) (OA), 1-octadecene (ODE, 90%), chlorin e6 (Ce6), polyallylamine (PAAm), 1,3-diphenylisobenzofuran (DPBF), dimethyl formamide (DMF), mPEG-succinimidyl carbonate (mPEG-SC), 1-ethyl-3-(3-dimethylaminopropyl)carbodiimide (EDC) and *N*-hydroxy-succinimide (NHS) were all purchased from Sigma-Aldrich. 4′,6′-Diamidino-2-phenylindole (DAPI) and paraformaldehyde (4%) were purchased from Beyotime Institute of Biotechnology. Dimethylformamide (DMF), NaOH and NH_4F were purchased from Beijing Chemical Works. All other chemical reagents were of analytical grade and were used directly without further purification. The Lewis lung cancer (LLC) cells and the human lung cancer (A549) cells were obtained from the College of Basic Medical Sciences, Jilin University. The cultured RPMI 1640 medium and fetal bovine serum (FBS) were obtained from Dingguo Biotechnology Development (China).

2.2 Preparation of UCNP-Ce6/PEG nano-photosensitizers

β-$NaErF_4$@$NaLuF_4$ core–shell UCNPs were synthesized following a previous report.[31] To obtain amino-functionalized UCNPs (NH_2-UCNPs), a ligand exchange method[32] was adopted by using PAAm to transfer the four hydrophobic as-synthesized UCNPs to the hydrophilic ones. Taking CS1 UCNPs as an example, 50 μL PAAm (20 wt%) aqueous solution was added to 4 mL ethanol, then 0.2 mL UCNPs (2 mg mL^{-1}) were added to the above solution and stirred overnight at room temperature. Finally, the obtained NH_2-UCNPs were further purified by centrifugation and redispersed in DMF for further use.

Next, for conjugating with Ce6, 5 mL of DMF solution, containing 0.2 mg of Ce6, 1 mg of EDC, and 1 mg of NHS, were stirred at room temperature for 2 h. Then, 20 mg of NH_2-UCNPs were added to the above solution for another 12 h. Finally, the UCNP-Ce6 nanophotosensitizers (nanoPSs) were purified by centrifugation and washed with DMF and water three times to remove the free Ce6 molecules. After that, PEG-SC was modified on the surface of UCNP-Ce6 to enhance its biocompatibility. Briefly, 2 mg of mPEG-SC, 2 mg of EDC, 2 mg of NHS and 10 mg of UCNP-Ce6 were added to 5 mL of DMF and stirred for 12 h. The products were centrifuged and dispersed in PBS solution. Similarly, the other UCNP-Ce6/PEG nanoPSs were obtained.

2.3 Singlet oxygen detection of samples

The optimum thickness of the shell was confirmed by the generation of singlet oxygen. The production of singlet oxygen was determined by the absorption of DPBF.[33] 10 μL of DPBF–ethanol solution (8 mM) was added to 2 mL of UCNP-Ce6/PEG solution (5 mg mL^{-1}). Then four mixtures were irradiated using an 800 nm laser at the same power density (0.68 W cm^{-2}), respectively. The absorption of DPBF at 417 nm was measured every 2 minutes.

2.4 MTT assays for cytotoxicity

The cells were seeded in a 96-well plate (1×10^4 cells per well) and incubated at 37 °C for 24 h. After removing the old medium, 100 μL fresh medium containing different concentrations (0, 50, 100, 200, 400 or 800 μg mL^{-1}) of UCNP-Ce6/PEG were added to each well and cultivated for another 24 h. For dark cytotoxicity, an MTT solution (20 μL, 5 mg mL^{-1}) was added into each well. After incubation for 6 h, the MTT solution was replaced with 150 μL DMSO in each well. The absorbance at 490 nm was measured using a microplate reader. For

Published on 04 April 2018. Downloaded by Changchun Institute of Optics, Fine Mechanics and Physics, CAS on 8/8/2019 8:17:54 AM.

PDT, the A549 cells were irradiated with an 800 nm laser (0.68 W cm^{-2}) for 15 min and 3 min intervals of each group. After another 24 h culture, the PDT effect was confirmed by a similar MTT method.

2.5 UCL, MR and CT imaging *in vitro*

The A549 cells were seeded in confocal dishes at a concentration of 10^4 cells per dish. After incubation for 24 h at 37 °C with 5% CO_2, 100 μL of UCNP-Ce6/PEG (200 μg mL^{-1}) were added into the dish. Then, the cells were incubated for 6 h and washed with PBS solution to remove free UCNP-Ce6. Before applying to imaging, the cells were fixed in paraformaldehyde (4 wt%, 500 μL) for 10 minutes and washed with PBS three times. Then, the nuclei were stained with 1 mL of DAPI (0.1 μg mL^{-1}) for 10 minutes and washed three times with PBS solution. The images of the cells were performed using a modified confocal microscope (Nikon Confocal Microscope C2/C2si) equipped with an external 980 nm laser.

The *in vitro* MR imaging experiments were performed in a 3.0 T Philips MRI magnet. T_2 relaxation of UCNPs with different concentrations (16, 32, 64, 128, and 256 μM) was measured in a 3.0 T MR scanner. The r_2 relaxivity values were determined by the linear fitting of $1/T_2$ relaxation time (s^{-1}) at various concentrations. The *in vitro* CT imaging was tested using a Philips 64-slice CT scanner at a voltage of 120 kV. The UCNPs were diluted into various concentrations (1.3, 2.6, 5.2, 10.5, and 21 mg ml^{-1}) and tested in the CT scanner. X-ray attenuation values for samples were finally calculated in Hounsfield units (HU) by averaging over the 3D based ROI.

2.6 MRI and CT imaging *in vivo*

As a proof of concept, the MRI and CT imaging were evaluated *in vivo*. The tumor-bearing mice were injected intravenously (IV) with NaCl solutions (0.9 wt%, 100 μL) containing desired amounts of UCNP-Ce6/PEG 10 mg mL^{-1} for MRI and CT imaging. The images were collected at the pre-injection and post-injection after 24 h.

2.7 Long-term toxicity assessment and anticancer studies *in vivo*

Animal experiments were conducted in accordance with the guidelines of the Regional Ethics Committee for Animal Experiments and were approved by the Institutional Animal Care and Use Committee of Jilin University. The C57BL/6 mice were purchased from Liaoning Changsheng Biotechnology Co. Ltd. The license number is SCXK(Liao) 20015-0001.

For long-term toxicity assessment of UCNP-Ce6/PEG nanoparticles, the C57BL/6 mice were treated with the as-mentioned NPs for 30 days and no injection of NPs was selected as the control group.

For anticancer studies, the mice were subcutaneously inoculated with Lewis lung cancer (LLC) cells (100 μL, 1×10^6 cells per mL). LLC tumor-bearing C57BL/6 mice (7–8 weeks) were weighed and randomly divided into 4 groups ($n = 5$). The mice were treated as below: (1) with PBS only (control group), (2) with NPs, (3) 800 nm laser only, (4) with NPs combined with 800 nm laser irradiation (treated group). All the mice were IV injected with various solutions. The laser treatment was done 5 times, each for 3 min with light irradiation at the same power density (0.5 W cm^{-2}). The therapeutic efficacy of NPs on the mice was assessed every other day for 14 days. The mice from the different groups were sacrificed after 14 days and their major organs (heart, liver, spleen, lung and kidney) and tumors were isolated.

All these tissues were stained with hematoxylin and eosin (H&E) to observe histological changes. The photographs were taken using an optical microscope.

3. Results and discussion

To acquire a high yield of cytotoxic $^1O_2$ for PDT, two aspects should be considered: the excitation intensity of light acting on photosensitizers and the LRET efficiency between UCNPs and photosensitizers. However, the shell thickness is a double-edged sword for the above aspects. On the one hand, a thicker shell can have a positive effect on enhancing the UCL. On the other hand, it increases the energy transfer (ET) distance between the activators (Er^{3+}) in the core and acceptors (Ce6 molecules modified on the surface), which has a negative effect on the ET efficiency. Thus, we tuned the shell thicknesses of $NaErF_4$@$NaLuF_4$ NPs to obtain an optimized PDT effect. The sizes of the $NaErF_4$ core and $NaErF_4$@$NaLuF_4$ core/shell UCNPs were measured by using a transmission electron microscope (TEM) and are given in Fig. 1, which were labelled as C, CS1, CS2, CS3 and CS4, respectively. With the gradual $NaLuF_4$ shell coating, we can see the corresponding increase in the particle size. The average NP diameters were determined to be 18 ± 0.5 nm (C), 23 ± 0.8 nm (CS1), 25 ± 1.2 nm (CS2), 28 ± 2.5 nm (CS3) and 33 ± 3.3 nm (CS4), respectively, which indicated that the average shell thicknesses were about 2.5 nm, 3.5 nm, 5 nm and 7.5 nm for CS1, CS2, CS3 and CS4, respectively. And the XRD patterns confirmed the hexagonal phase of the core/shell $NaErF_4$@$NaLuF_4$ NPs, as shown in Fig. 1f.

The four NPs mentioned above were decorated with functional ligands to further study the ET efficiency from the UCNPs to the photosensitizers. The hydrophilic NH_2-functionalized UCNPs (NH_2-UCNPs for short) were prepared *via* a ligand-exchange process using PAAm as the surface coating agent[34] and confirmed by the fluorescamine method[35] as shown in Fig. S1.† Then the NH_2-UCNPs were conjugated with Ce6 molecules whose –COOH groups enable the formation of amide bonds (CO–NH). The covalent conjugation of UCNPs with Ce6 was confirmed by the Fourier transform infrared (FTIR) spectra shown in Fig. S2.† After the conjugation, the peak appeared at 1660 cm^{-1} corresponding respectively to the C═O stretching vibration and N–H bending vibration modes of a secondary amide. The result confirmed that the UCNP-Ce6 nanoPSs were successfully obtained. Then the colloidal stability of UCNP-Ce6/PEG in phosphate buffered solutions was studied. As shown in Fig. S3,† a tiny fluctuation of the hydro-

 This journal is © The Royal Society of Chemistry 2018

Published on 04 April 2018. Downloaded by Changchun Institute of Optics, Fine Mechanics and Physics, CAS on 8/8/2019 8:17:54 AM.

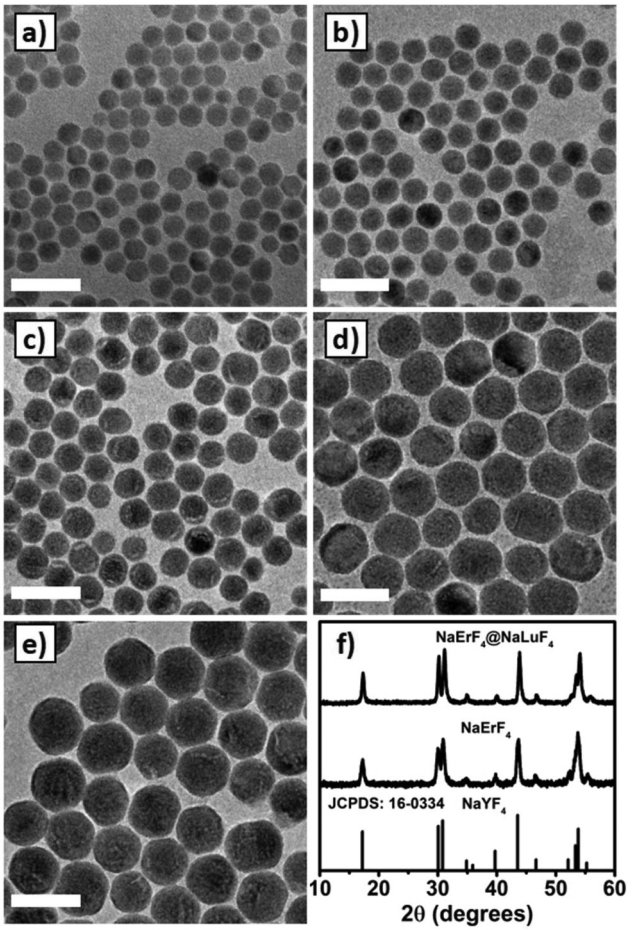

Fig. 1 TEM images of (a) the $NaErF_4$ core, and core–shell structured $NaErF_4$@$NaLuF_4$ of (b) CS1, (c) CS2, (d) CS3, (e) CS4. All the scale bars are 100 nm. (f) XRD patterns of core $NaErF_4$, core–shell $NaErF_4$@$NaLuF_4$ UCNPs and the standard pattern of β-$NaYF_4$ for comparison.

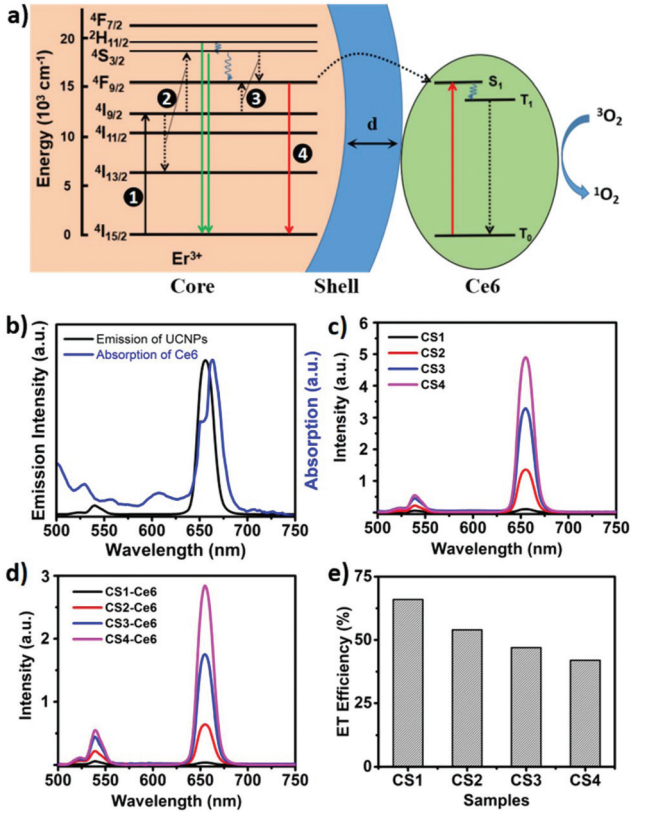

Fig. 2 (a) Schematic diagram of the upconversion process in the UCNP-Ce6 nanoconjugate under 800 nm excitation, and the energy transfer between UCNPs and Ce6. (b) The overlap of the absorption of the Ce6 photosensitizer and the emission of $NaErF_4$@$NaLuF_4$ UCNPs. The emission spectra of (c) UCNPs and (d) UCNP-Ce6 samples with changed shell thickness. (e) ET efficiency of the four as-obtained UCNP-Ce6 samples.

dynamic diameter demonstrated that the sample could be stable within 96 h.

The mechanism of LRET upon 800 nm excitation is shown in Fig. 2a. The $^4I_{9/2}$ level of Er^{3+} is populated from the $^4I_{15/2}$ level by direct absorption of 800 nm (ground state absorption, GSA), and the population of $^4S_{3/2}$ can be attributed to the efficient cross relaxation (CR) interaction between the up-closed Er^{3+} ions: $2^4I_{9/2} \rightarrow {}^4S_{3/2} + {}^4I_{13/2}$. Then, the electrons can decay non-radiatively from the $^2H_{11/2}$ level to the $^4S_{3/2}$ level, resulting in the green emission bands from 520 nm to 540 nm. Subsequently, the CR process: $^4S_{3/2} + {}^4I_{9/2} \rightarrow 2^4F_{9/2}$ leads to an efficient ET from the green emission band to the red emission band, and therefore causes a relatively high red/green emission ratio. Because UC processes involve interactions between multi-energy levels, the UC emission intensity exhibits a unique non-linear excitation power-dependent characteristic, as indicated in Fig. S4.† Furthermore, because of the absorption band (625–700 nm) of the Ce6 molecules overlapping well with the red emission band of UCNPs, the energy transfer may occur from UCNPs to Ce6 molecules (Fig. 2b). Indeed, after binding with the Ce6 molecules, the UCNPs are all observed with a decreased red emission intensity, due to the ET from the UCNPs to the photosensitizer (Fig. 2c and d). The ET efficiency of this process can be calculated from the reduced value of donor luminescence intensity and is given by $\eta = (I - I')/I$, where I and I' are emission intensities of the donor in the absence and presence of the acceptor, respectively. Obviously, due to the prolonged ET distance, the ET efficiency decreased monotonically from 66% (sample CS1) to less than 50% (sample CS4), as shown in Fig. 2e.

To further validate the ET process from UCNPs to Ce6 molecules, we monitored the time evolution of the red upconversion emission of these samples under 800 nm pulse excitation, as shown in Fig. 3. The shortened luminescence lifetime of donors was another piece of evidence of the ET process between donors and acceptors.[36,37] We can find that the decay time of the 655 nm emission becomes longer when the shell becomes thicker because of the effective passivation of surface defects. And the 655 nm emission decay time of UCNP-Ce6 nanoPSs was shorter than that of the four corres-

Published on 04 April 2018. Downloaded by Changchun Institute of Optics, Fine Mechanics and Physics, CAS on 8/8/2019 8:17:54 AM.

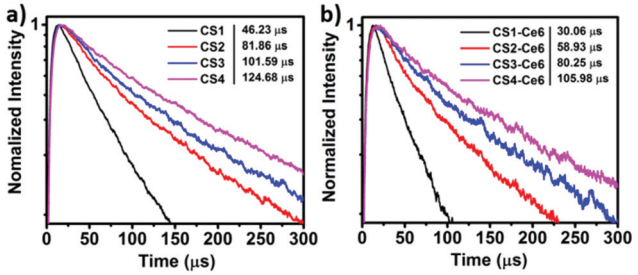

Fig. 3 Time evolution of UC luminescence at 655 nm under 800 nm excitation of (a) a set of UCNPs and (b) UCNP-Ce6. Inset: decay times are calculated by biexponential fits of the 655 nm emission.

ponding UCNPs. All these results confirmed the presence of the ET process from UCNPs to Ce6 molecules.

The optimum thickness of the shell was determined through the generation of singlet oxygen, which was evaluated by the consumption of a 3-diphenylisobenzofuran (DPBF) probe. It is achieved by monitoring the absorption drop-off rate at 417 nm of the DPBF probe with the exposure time accumulation every 2 minutes under CW 800 nm irradiation. In order to exclude the interference from the Ce6 absorption at 417 nm, the monitored spectra were subtracted by the Ce6 absorption reference. All four kinds of UCNP-Ce6/PEG samples were observed with an obvious decrease in the peaks at 417 nm, showing the consumption of the DPBF probe as the exposure time increases, as shown in Fig. 4a–d. The consumption rate of the four samples (Fig. 4e) indicates the capacity of producing $^1O_2$ in the sample solutions. We could see that the sample of CS3-Ce6 (18 nm core and 5 nm shell) was the best one for $^1O_2$ generation, although this sample shows neither the strongest UCL nor the highest ET efficiency.

Before applying the UCNPs (CS3) to biological applications, we evaluated the dark cytotoxicity of various concentrations of the UCNP-Ce6/PEG sample against the A549 cells using the MTT assay, as shown in Fig. 5. The results demonstrated that there was no significant decrease in cell viability (>90%) below the concentration of 200 μg mL^{-1}. Subsequently, we evaluated the PDT effect of the corresponding concentration under 800 nm NIR laser irradiation at 0.68 W cm^{-2} for 15 min. The cell viability dramatically decreased to 26% at the same concentration, which illustrated their NIR-induced cancer cell killing ability. In order to study the long-term toxicity of UCNP-Ce6/PEG, the mice were intravenously treated with the sample for 30 days and then the histological results of the main organs revealed no pathological changes in the heart, lung, kidney, liver or spleen, compared with the control group (Fig. S5†). It further demonstrates that the UCNP-Ce6/PEG nanoPSs with the optimum $NaLuF_4$ shell thickness (5 nm) can be potentially used for 800 nm phototriggered therapy.

Apart from the therapy function, UCNPs can perfectly provide a functional imaging nanoplatform for diagnostic and imaging-guided therapy, in which the ability of multimodality imaging is highly valued. Next, we turn to evaluate the multimodality imaging performance of CS3. For optical imaging, the near-infrared region (700–1000 nm) is more desirable than the visible region (450–700 nm), which shows a higher penetration depth for optical imaging.[38,39] Herein, the $NaErF_4$@$NaLuF_4$ UCNPs allow an excellent imaging due to

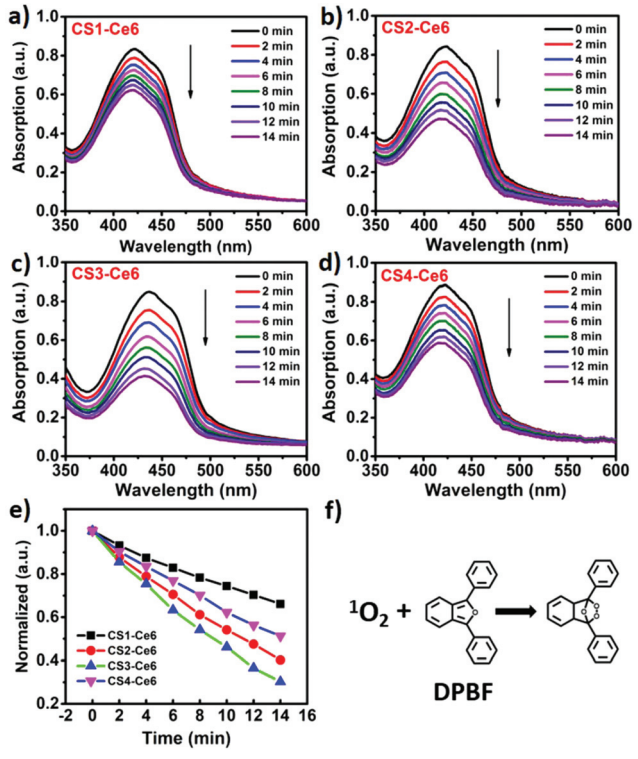

Fig. 4 (a–d) Time dependence of absorption of CS1–CS4 four samples under 800 nm excitation; (e) absorption at 417 nm of DPBF in the solutions of four samples as a function of irradiation time; (f) sketch map of the oxidation reaction process of DPBF by $^1O_2$.

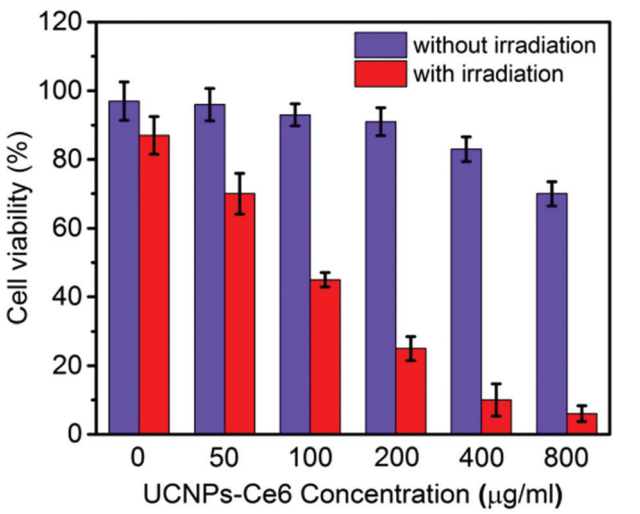

Fig. 5 Viability of A549 cells incubated with UCNP-Ce6/PEG at different concentrations with (red) or without (purple) 800 nm irradiation for PDT.

This journal is © The Royal Society of Chemistry 2018

Published on 04 April 2018. Downloaded by Changchun Institute of Optics, Fine Mechanics and Physics, CAS on 8/8/2019 8:17:54 AM.

their stronger emission around 800 nm under 980 nm laser excitation (NIR-to-NIR) (Fig. S6†).

Fig. 6 presents the *in vitro* optical imaging of CS3-Ce6/PEG nanoPSs, incubated with A549 cells after 6 h incubation. The nuclei were stained with DAPI, showing a blue color (Fig. 8b) and the red color represented the invisible near-infrared emission of 800 nm from the CS3-Ce6/PEG nanoPSs (Fig. 6c). We can see that the morphology of the nuclei was not altered, indicating the good activity of the treated cells. As shown in the overlay image in Fig. 6d, the red emission of UCNP-Ce6/PEG was in the cytoplasmic region and around the nuclear region (in blue), implying that the UCNPs have been internalized into the living cells. Therefore, the results above present as a strong proof that the UCNP-Ce6/PEG sample can work well in the optical imaging mode.

With the intrinsic magnetic properties of Er^{3+} ions, Er^{3+}-based materials are promising T_2 relaxation contrast agents (CAs) for MRI. However, due to the concentration quenching effect, the activators (Er^{3+}) of UCNPs are usually doped at a low doping level, which substantially restricts its MRI application. Though the $NaErF_4$:30% Yb nanorods have been reported as CAs for T_2-weighted MRI, the surface defect could not be passivated, resulting in a low UCL intensity.[40] Beyond that, the large scale of these nanorods with a length of 810 nm and diameter of 115 nm was unfavorable for biological application (<100 nm).[41] The shell epitaxial growth technique makes the $NaErF_4$@$NaLuF_4$ nanostructure highly efficient in UCL with a grain size of about 28 nm. And as an MRI candidate, its T_2 relaxation performance was studied and is given in Fig. 7a. The pattern, representing the signal intensity of MR, gradually darkens with the increasing concentration of the UCNP-Ce6/PEG sample. The MR parameter (r_2), determined by the slope of the relaxation rate ($1/T_2$) with different concentrations, was 9.16 s^{-1} mM^{-1} at 3.0 T. The results indicated that the $NaErF_4$@$NaLuF_4$ nanomaterials are excellent contrast agents for high-field T_2-weighted MRI.

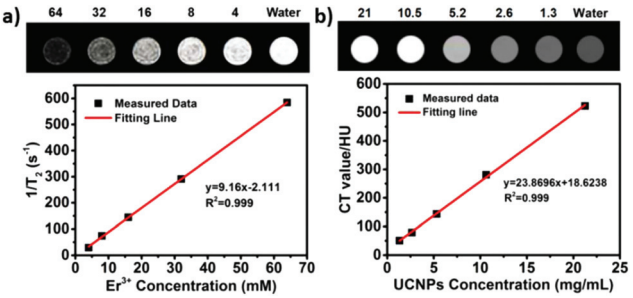

Fig. 7 (a) T_2-Weighted MR images and relaxation rates, (b) CT images and CT (HU) values of the UCNP-Ce6 aqueous dispersions at the indicated concentrations.

Moreover, due to the large K-edge energy of Er^{3+} and Lu^{3+}, it can be expected that the $NaErF_4$@$NaLuF_4$ nanomaterial also has potential in X-ray-based imaging. Fig. 7b shows the potency of UCNPs to be used as X-ray CT CAs. As presented, with the increase of mass concentrations, the CT signal increased obviously and CT values (HU) showed a positive enhancement with a large slope of 23.86, which was better than the 17.5 of commercial iopromide.[42] These findings confirm that the $NaErF_4$@$NaLuF_4$ nanomaterial is a promising multimodality imaging nanoplatform for precise diagnosis and therapy.

As a proof-of-concept, the MRI and X-ray CT contrast capability of the UCNP-Ce6/PEG were evaluated *in vivo*. UCNP-Ce6/PEG solutions (100 μL, 10 mg mL^{-1}) were injected intravenously into tumor-bearing mice. As expected, in T_2-MR images (Fig. 8a and b), the tumor area became darker after 24 h post-injection, which agreed with the *in vitro* results. In addition, a signal enhancement was found in the CT images 24 h post-injection, as shown in Fig. 8c and d. The experimental results suggest that the UCNP-Ce6/PEG photosensitizers are highly accumulated in the tumor because of the enhanced permeability and the retention (EPR) effect.

On the basis of the MRI and CT results, we further evaluated the efficacy of 800 nm laser triggered therapy *in vivo*. The LLC tumor-bearing C57BL/6 mice were treated with the intravenous injection of UCNP-Ce6/PEG. After that, the tumors were irradiated with an 800 nm laser (0.5 W cm^{-2}) for 3 min 5 times every day. After 14 days treatment, the results are shown in Fig. 9. We can see that the tumor size of the control group was robustly larger than the size of the group injected with UCNP-Ce6/PEG under 800 nm irradiation (Fig. 9a and b), and the relative volume of the tumors is shown in Fig. S7.† Furthermore, the tumor histological section of the control group and the treated group are presented in Fig. 9c. Compared with the control group, the number of apoptotic and necrotic tumor cells has greatly increased in the treated group. All these

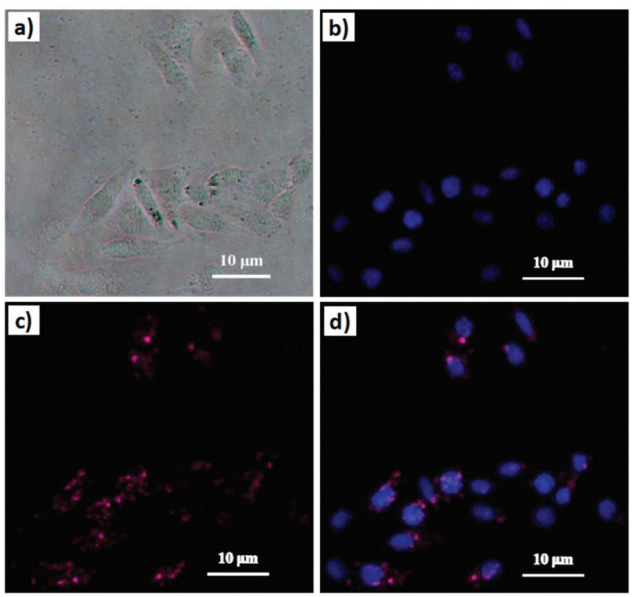

Fig. 6 *In vitro* UCL images of A549 cells incubated with 200 μg mL^{-1} UCNP-Ce6 for 6 h at 37 °C. (a) Bright channel; (b) blue channel: DAPI signals were collected at 450–500 nm; (c) NIR channel: UCL signals were collected at 750–850 nm (false magenta color); (d) overlay of the NIR field and blue field.

Published on 04 April 2018. Downloaded by Changchun Institute of Optics, Fine Mechanics and Physics, CAS on 8/8/2019 8:17:54 AM.

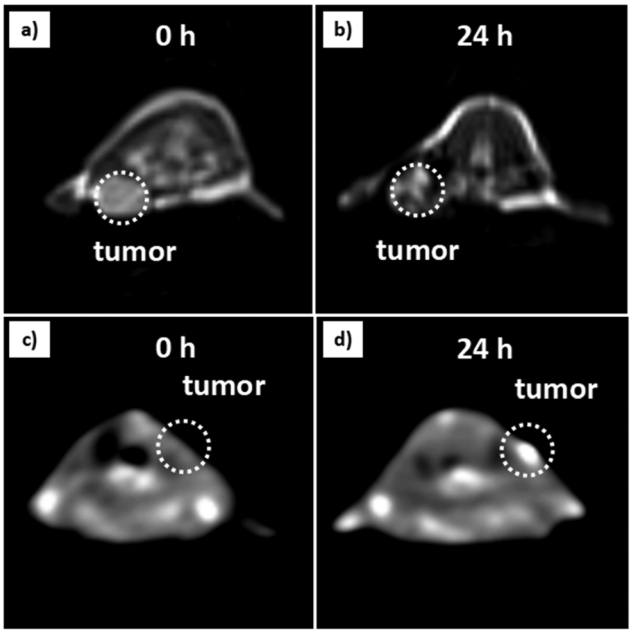

Fig. 8 *In vivo* (a–b) T_2-MR and (c–d) coronal CT images of the tumor after intravenous injection of UCNP-Ce6/PEG before and 24 h after injection, respectively.

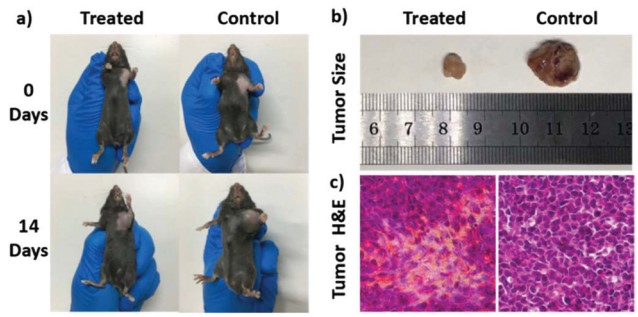

Fig. 9 (a) The photos of the control and treated mice before and after 14 days of treatment. (b) The tumor size was obtained after treatment. (c) The tumor H&E stained images of treated mice (left) and control mice (right).

results demonstrate that UCNP-Ce6/PEG with 800 nm irradiation has an obvious inhibitory effect on tumor growth. In addition, the histological assessment of the heart, liver, spleen, lung and kidney organs from the control and treated groups are shown in Fig. S8.† It can be seen that no obvious pathological changes of the major organs were observed in the treated group, indicating negligible systemic toxicity. Herein, our results demonstrated that UCNP-Ce6/PEG is a highly promising nanoconjugate for use in the PDT treatment of tumors.

4. Conclusion

In summary, we have synthesized a new near-infrared 800 nm driven nanoconjugate for multimodality imaging and photodynamic therapy, composed of core–shell structured $NaErF_4$@$NaLuF_4$ UCNPs and covalently coupled Ce6 photosensitizers. For 800 nm triggered PDT, a 5 nm thickness of the $NaLuF_4$ shell was a priority for $^1O_2$ generation. In this system, the T_2 relaxation rate of Er^{3+} ions can be exploited for MRI contrast agents with a r_2 value of 9.16 s^{-1} $mmoL^{-1}$, and both Er^{3+} and Lu^{3+} ions can provide large X-ray attenuation with a slope of 23.86 for CT imaging. A satisfying capability of multimodality imaging including UCL, MR and CT imaging was convincingly demonstrated. The employed $NaErF_4$@$NaLuF_4$ nanomaterial solves the problem of the mutual influence of UCNPs in multimodality imaging within a simple core/shell structure, and provides new NIR 800 nm driven nanomaterials to reduce the thermal effect problem.

Conflicts of interest

There are no conflicts to declare.

Acknowledgements

This work was financially supported by the NSF of China (11374297, 61575194, 11674316, 11504371, 11471278 and 11604331), the Project of Science and Technology Agency, Jilin Province (20170520113JH, 20170520112JH, 20170519002JH and 20180101222JC) and the open project in 2016 supported by the State Key Laboratory of Luminescence and Applications.

Notes and references

1 G. Tian, X. Zhang, Z. J. Gu and Y. L. Zhao, *Adv. Mater.*, 2015, **27**, 7692–7712.
2 G. Chen, H. Qju, P. N. Prasad and X. Chen, *Chem. Rev.*, 2014, **114**, 5161–5214.
3 H. Dong, S. R. Du, X. Y. Zheng, G. M. Lyu, L.-D. Sun, L. D. Li, P. Z. Zhang, C. Zhang and C. H. Yan, *Chem. Rev.*, 2015, **115**, 10725–10815.
4 A. Escudero, A. I. Becerro, C. Carrillo-Carrion, N. O. Nunez, M. V. Zyuzin, M. Laguna, D. Gonzalez-Mancebo, M. Ocana and W. J. Parak, *Nanophotonics*, 2017, **6**, 881–921.
5 J. Xu, P. Yang, M. Sun, H. Bi, B. Liu, D. Yang, S. Gai, F. He and J. Lin, *ACS Nano*, 2017, **11**, 4133–4144.
6 S. He, N. J. J. Johnson, V. A. Nguyen Huu, E. Cory, Y. Huang, R. L. Sah, J. V. Jokerst and A. Almutairi, *Nano Lett.*, 2017, **17**, 4873–4880.
7 Z. Yi, X. Li, Z. Xue, X. Liang, W. Lu, H. Peng, H. Liu, S. Zeng and J. Hao, *Adv. Funct. Mater.*, 2015, **25**, 7119–7129.
8 Z. Gao, T. Ma, E. Zhao, D. Docter, W. Yang, R. H. Stauber and M. Gao, *Small*, 2016, **12**, 556–576.
9 J. J. He, W. Zheng, F. L. Ligmajer, C. F. Chan, Z. Y. Bao, K. L. Wong, X. Y. Chen, J. H. Hao, J. Y. Dai, S. F. Yu and D. Y. Lei, *Light: Sci. Appl.*, 2017, **6**, e16217.

 This journal is © The Royal Society of Chemistry 2018

Published on 04 April 2018. Downloaded by Changchun Institute of Optics, Fine Mechanics and Physics, CAS on 8/8/2019 8:17:54 AM.

10 J. Zuo, L. Tu, Q. Li, Y. Feng, I. Que, Y. Zhang, X. Liu, B. Xue, L. J. Cruz, Y. Chang, H. Zhang and X. Kong, *ACS Nano*, 2018, **12**, 3217–3225.
11 M. Guan, H. Dong, J. Ge, D. Chen, L. Sun, S. Li, C. Wang, C. Yan, P. Wang and C. Shu, *NPG Asia Mater.*, 2015, **7**, e205.
12 M. Hu, D. D. Ma, Y. Z. Cheng, C. C. Liu, Z. P. Zhang, Y. J. Cai, S. Wu and R. F. Wang, *J. Mater. Chem. B*, 2017, **5**, 2662–2670.
13 Q. Zhan, J. Qian, H. Liang, G. Somesfalean, D. Wang, S. He, Z. Zhang and S. Andersson-Engels, *ACS Nano*, 2011, **5**, 3744–3757.
14 D. Wang, B. Xue, X. G. Kong, L. P. Tu, X. M. Liu, Y. L. Zhang, Y. L. Chang, Y. S. Luo, H. Y. Zhao and H. Zhang, *Nanoscale*, 2015, **7**, 190–197.
15 Y. Sun, X. J. Zhu, J. J. Peng and F. Y. Li, *ACS Nano*, 2013, **7**, 11290–11300.
16 X. D. Wang, R. R. Valiev, T. Y. Ohulchanskyy, H. Agren, C. H. Yang and G. Y. Chen, *Chem. Soc. Rev.*, 2017, **46**, 4150–4167.
17 J. Xu, P. Yang, M. Sun, H. Bi, B. Liu, D. Yang, S. Gai, F. He and J. Lin, *ACS Nano*, 2017, **11**, 4133–4144.
18 S. Hao, G. Chen, C. Yang, W. Shao, W. Wei, Y. Liu and P. N. Prasad, *Nanoscale*, 2017, **9**, 10633–10638.
19 B. Xu, X. Zhang, W. Huang, Y. Yang, Y. Ma, Z. Gu, T. Zhai and Y. Zhao, *J. Mater. Chem. B*, 2016, **4**, 2776–2784.
20 L. Tu, X. Liu, F. Wu and H. Zhang, *Chem. Soc. Rev.*, 2015, **44**, 1331–1345.
21 N. J. J. Johnson, S. He, S. Diao, E. M. Chan, H. Dai and A. Almutairi, *J. Am. Chem. Soc.*, 2017, **139**, 3275–3282.
22 Q. Chen, X. Xie, B. Huang, L. Liang, S. Han, Z. Yi, Y. Wang, Y. Li, D. Fan, L. Huang and X. Liu, *Angew. Chem., Int. Ed.*, 2017, **56**, 7605–7609.
23 J. Zuo, Q. Q. Li, B. Xue, C. X. Li, Y. L. Chang, Y. L. Zhang, X. M. Liu, L. P. Tu, H. Zhang and X. G. Kong, *Nanoscale*, 2017, **9**, 7941–7946.
24 Y. Wang, K. Liu, X. Liu, K. Dohnalova, T. Gregorkiewicz, X. Kong, M. C. G. Aalders, W. J. Buma and H. Zhang, *J. Phys. Chem. Lett.*, 2011, **2**, 2083–2088.
25 D. Wang, B. Liu, Z. Quan, C. Li, Z. Hou, B. Xing and J. Lin, *J. Mater. Chem. B*, 2017, **5**, 2209–2230.
26 F. Wang and X. Liu, *Chem. Soc. Rev.*, 2009, **38**, 976–989.
27 X. Ding, J. H. Liu, D. P. Liu, J. Q. Li, F. Wang, L. J. Li, Y. H. Wang, S. Y. Song and H. J. Zhang, *Nano Res.*, 2017, **10**, 3434–3446.
28 S. Viswanathan, Z. Kovacs, K. N. Green, S. J. Ratnakar and A. D. Sherry, *Chem. Rev.*, 2010, **110**, 2960–3018.
29 H. Wang, Z. Yi, L. Rao, H. Liu and S. Zeng, *J. Mater. Chem. C*, 2013, **1**, 5520–5526.
30 G. Pintacuda, M. John, X.-C. Su and G. Otting, *Acc. Chem. Res.*, 2007, **40**, 206–212.
31 H.-S. Qian and Y. Zhang, *Langmuir*, 2008, **24**, 12123–12125.
32 H. S. Qian, H. C. Guo, P. C.-L. Ho, R. Mahendran and Y. Zhang, *Small*, 2009, **5**, 2285–2290.
33 P. B. Merkel and D. R. Kearns, *J. Am. Chem. Soc.*, 1975, **97**, 462–463.
34 L. Xia, X. Kong, X. Liu, L. Tu, Y. Zhang, Y. Chang, K. Liu, D. Shen, H. Zhao and H. Zhang, *Biomaterials*, 2014, **35**, 4146–4156.
35 S. H. Liu and M. Y. Han, *Adv. Funct. Mater.*, 2005, **15**, 961–967.
36 A. Bednarkiewicz, M. Nyk, M. Samoc and W. Strek, *J. Phys. Chem. C*, 2010, **114**, 17535–17541.
37 Y. Ding, F. Wu, Y. Zhang, X. Liu, E. M. L. D. de Jong, T. Gregorkiewicz, X. Hong, Y. Liu, M. C. G. Aalders, W. J. Buma and H. Zhang, *J. Phys. Chem. Lett.*, 2015, **6**, 2518–2523.
38 J. Zhou, Z. Liu and F. Li, *Chem. Soc. Rev.*, 2012, **41**, 1323–1349.
39 Z. Li, Y. Zhang, H. La, R. Zhu, G. El-Banna, Y. Wei and G. Han, *Nanomaterials*, 2015, **5**, 2148–2168.
40 H. Wang, W. Lu, T. Zeng, Z. Yi, L. Rao, H. Liu and S. Zeng, *Nanoscale*, 2014, **6**, 2855–2860.
41 H. Yin, H. P. Too and G. M. Chow, *Biomaterials*, 2005, **26**, 5818–5826.
42 D. M. Yang, Y. L. Dai, J. H. Liu, Y. Zhou, Y. Y. Chen, C. X. Li, P. A. Ma and J. Lin, *Biomaterials*, 2014, **35**, 2011–2023.